Two-dimensional droplet ripening in a concentration gradient

Paul C. Bressloff

Department of Mathematics, University of Utah, Salt Lake City, Utah 84112, USA

E-mail: `bressloff@math.utah.edu`

Abstract. The discovery of various membraneless subcellular structures (biological condensates) in the cytoplasm and nucleus of cells has generated considerable interest in the effects of non-equilibrium chemical reactions on liquid-liquid phase separation and droplet ripening. Examples include the suppression of droplet ripening due to ATP-driven protein phosphorylation and the spatial segregation of droplets due to regulation by protein concentration gradients. Most studies of biological phase separation have focused on 3D droplet formation, for which mean field methods can be applied. However, mean field theory breaks down in the case of 2D systems, since the concentration around a droplet varies as $\ln R$ rather than R^{-1}, where R is the distance from the center of a droplet. In this paper we use the asymptotic theory of diffusion in domains with small holes or exclusions (strongly localized perturbations) to study the segregation of circular droplets in gradient systems. We proceed by partitioning the region outside the droplets into a set of inner regions around each droplet together with an outer region where mean-field interactions occur. Asymptotically matching the inner and outer solutions, we derive dynamical equations for the position-dependent growth and drift of droplets. We thus show how a gradient of regulatory proteins leads to the segregation of droplets to one end of the domain, as previously found for 3D droplets.

1. Introduction

In classical liquid-liquid phase separation a homogeneous solution separates into two coexisting liquid phases with different densities, a high density phase ϕ_b and a low density phase ϕ_a. If the original solution is thermodynamically unstable, then the kinetics of phase separation involves rapid demixing due to the absence of a nucleation barrier (spinodal decomposition). Early stages of phase separation involve the formation of microscopic solute-rich domains dispersed throughout the liquid, which subsequently grow and coalesce to form macroscopic clusters or droplets. Eventually the total volume of droplets stabilizes, and the late stage of phase separation is characterized by a coarsening process known as Ostwald ripening [19]. This is a diffusion-driven process whereby droplets larger (smaller) than a critical radius R_c grow (shrink), with R_c itself an increasing function of time, so that ultimately only a single droplet remains. The diffusive exchange of material from a small droplet to a large droplet is due to the fact that interfacial tension increases the local concentration in a neighborhood of a droplet according to the Gibbs-Thompson law; such an increase is inversely proportional to the droplet radius according to $\phi(R) = \phi_a(1 + \ell_c/R)$ with ℓ_c the capillary length. The first quantitative formulation of Ostwald ripening was developed by Lifshitz and Slyozov [18] and Wagner [22], and is commonly referred to as classical LSW theory. A crucial assumption of LSW theory is that the interaction between droplets can be expressed solely through a common mean field, which determines the so-called supersaturation of the system. This mean field approximation exploits the fact that the concentration around a droplet varies as $1/r$, where r is the distance from the center of the droplet. However, mean field theory breaks down in the case of circular droplets in two-dimensional (2D) systems such as thin films, since the concentration around a droplet varies as $\ln r$ rather than r^{-1}. Thus, more care must be taken in imposing far-field conditions [1, 15].

There is now significant renewed interest in liquid-liquid phase separation and Ostwald ripening due to the discovery of membraneless subcellular structures (biological condensates) such as P granules in the cytoplasm and nucleoli in the nucleus of cells [4, 5, 28, 11, 14, 2, 3, 12, 17]. These structures consist of enhanced concentrations of various proteins and RNA in a localized domain, without a physical membrane separating it from the surrounding medium. Proteins are highly mobile within a biological condensate and are continually exchanged with the cytosol. Although liquid-liquid phase separation is emerging as the key organizing principle underlying the formation of biological condensates, the classical theory has been modified in order to take into account the fact that biological phase separation can be regulated by active processes such as non-equilibrium chemical reactions. Examples include the suppression of Ostwald ripening due to ATP-driven protein phosphorylation [29, 27] and the spatial segregation of droplets due to regulation by protein concentration gradients [25, 26].

Almost all current theoretical studies of biological phase separation have focused on 3D spherical droplets, for which mean field approximations hold. However, there are also examples of phase separation in quasi-2D domains, such as the clustering of curvature-inducing proteins that regulate cell shape [13]. Moreover, polarized crawling cells such as keratocytes and fibroblasts are highly flattened and often treated as 2D systems. 2D active emulsions (thin films) are also of considerable interest within the wider physics community [26]. Recently, we have shown how asymptotic methods can be used to study the suppression of Ostwald ripening in a 2D solution undergoing active

liquid-liquid phase separation [7]. In this paper, we extend these methods to the case of 2D droplet ripening in a concentration gradient. We assume that droplets are well separated with mean separation d and characteristic radius R such that $R/d = O(\epsilon)$ for $0 < \epsilon \ll 1$. We solve the quasi-steady-state diffusion equation by partitioning the region outside the droplets into a set of inner regions around each droplet together with an outer region where mean-field interactions occur. The inner and outer solutions are matched by carrying out an asymptotic expansion in $\nu = -1/\ln \epsilon$. Using a separation of time scales, we then derive leading order dynamical equations for the position-dependent growth and drift velocity of the droplets. We also show how finite-size effects can be incorporated into the theory by including higher-order terms in the asymptotic expansion, which depend on the positions of the droplets and the boundary of the 2D domain.

2. Phase separation in a concentration gradient

Protein concentration gradients play an important role during asymmetric cell division of the *C. elegans* zygote. Within the context of biological condensates, it has been found that RNA-protein aggregates in the form of so-called P-granules are segregated to the posterior side of the cell, and are located in the posterior daughter cell after division. Moreover, the segregation and ripening of P-granule droplets is driven by the concentration gradient of a regulatory protein known as Mex-5 [4, 16, 20]. This has motivated a theoretical study of 3D droplet ripening in a protein concentration gradient, where both the supersaturation and low density phase concentration are taken to be position dependent [25, 26]. Here we briefly describe the underlying model.

Let R denote the regulatory protein and P denote the solute that undergoes phase separation in a solvent S. The basic regulatory mechanism is taken to be the binding of R to P, which forms a complex C that cannot phase separate:

$$R + P \underset{h}{\overset{k}{\rightleftharpoons}} C. \tag{2.1}$$

This has the effect of reducing the volume fraction of solute molecules that can participate in phase separation. Let ϕ denote the total volume fraction of solute, which is given by the sum of contributions from bound (ϕ_C) and free (ϕ_P) molecules,

$$\phi = \phi_P + \phi_C.$$

If ϕ_S and ϕ_R denote the volume fraction of solvent and free regulator, respectively, then $\phi + \phi_S + \phi_R = 1$. We will assume that $\phi_R \ll 1$ (dilute regulator concentration) so that $\phi + \phi_S \approx 1$. Assuming local equilibrium of the fast binding reactions, and taking the molecular volumes of C and P to be the same, $v_C = v_P = v$, we have $k\phi_P\phi_R/v_R = h\phi_C$, where v_R is the molecular volume of R molecules and ϕ_R is the corresponding volume fraction. Hence,

$$\phi_P = \frac{\phi}{1 + K\phi_R}, \quad K = \frac{k}{hv_R}.$$

In order to explore the consequences of this binding reaction on phase separation, consider the classical free energy density of the ternary solution [10]:

$$f(\phi; \phi_R) = k_B T \left[\frac{1}{v} \phi \ln \phi + \frac{1}{v_S}(1 - \phi) \ln(1 - \phi) + \chi \frac{\phi}{1 + K\phi_R}(1 - \phi) \right], \tag{2.2}$$

where v_S is the molecular volume of solvent, and χ is the effective interaction energy. For simplicity, we ignore the mixing entropy of the complex C and only consider interaction energies between P and S. It follows that the only dependence of the free energy on the regulator volume fraction ϕ_R is via its dependence on ϕ_P. Note that the interaction energy term can be expressed as [25, 26]

$$\mathcal{E} = k_B T \chi_{\text{eff}} \phi(1-\phi), \quad \chi_{\text{eff}} = \chi \left(1 - \frac{K\phi_R}{1+K\phi_R} \right). \tag{2.3}$$

It follows that increasing the regulator concentration ϕ_R leads to a decrease in the effective interaction parameter χ_{eff}.

The free energy density $f(\phi; \phi_R)$ for fixed ϕ_R has a single minimum for sufficiently small χ_{eff} but switches to two local minima $\phi_{a,b}$ as χ_{eff} crosses a critical point χ_c. If one now plots the coexistence curves for ϕ_a and ϕ_b in the ϕ-ϕ_R plane, one finds that changing ϕ_R moves the system to different points in the phase diagram, which is how the regulator protein can control phase separation. In particular, suppose that there exists a spatially varying concentration gradient $\phi_R(\mathbf{r})$ that, for simplicity, varies linearly in the x-direction, $\phi_R(\mathbf{r}) = \phi_R(0) - bx$. It immediately follows that χ_{eff} and hence $\phi_{a,b}$ become x-dependent, as illustrated in Fig. 1. One major simplification is to take $v_S \gg v$ so that the volume fraction ϕ_b of the high density phase is approximately independent of x. One can then focus on determining the spatially varying volume fraction ϕ outside the droplets along the lines of Weber *et al.* [25, 26]. These authors extend the classical mean field theory of droplet ripening by considering the effects of a spatially varying volume fraction $\phi_a(x)$ and a time-dependent, spatially varying far-field $\phi_\infty(x,t)$ that represents the collective effects of surrounding droplets. In classical LSW theory, the far field ϕ_∞ is spatially uniform during late-stage ripening, assuming that the mean separation d between droplets satisfies $d \gg R$, where R is the mean droplet radius. Under the further separation of length scales $R \ll d \ll L$,
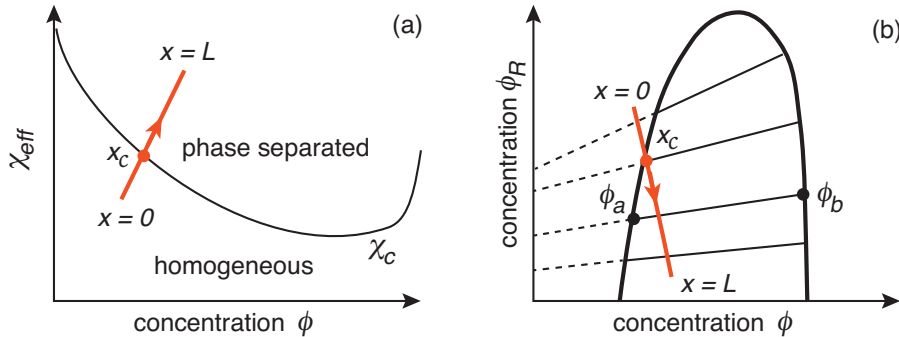

Figure 1: Effect of a linearly decreasing regulator concentration $\phi_R(x)$ on phase separation, $x \in [0, L]$. (a) Sketch of phase transition curve $\chi_{\text{eff}} = \chi_c$ for phase separation as a function of ϕ. The variation of χ_{eff} with x traces a straight line in the phase diagram that crosses the critical curve at position x_c. (b) Coexistence curves in the (ϕ, ϕ_R)-plane for total solute concentration ϕ and regulator concentration ϕ_R. The thin straight lines link points within the phase separation region to the corresponding low and high density phases $\phi_{a,b}$ on the coexistence curve. As the position x varies, there is a corresponding change in ϕ_R, which places the system at different points in the phase diagram (red curve). Droplets can only form at points that lie within the coexistence curve. The position x_c marks the boundary between droplet formation and dissolution.

where L is the system size, one can partition the system into local regions with a size corresponding to the intermediate length scale d. Droplets in a local domain around a spatial position x will have coexisting equilibrium concentrations $\phi_a(x), \phi_b$ provided that the point $(\phi, \phi_R(x))$ is located inside the phase separation region of the associated phase diagram, see Fig. 1. Finally, if the common far field concentration within the local region is $\phi_\infty(x, t)$, then one can define a spatio-temporal dependent supersaturation $\Delta(x, t) = \phi_\infty(x, t) - \phi_a(x)$ and use this to analyze the dynamics of droplets by modifying classical LSW theory [25, 26]. Since the quasi-steady-state local solute concentration is not radially symmetric, one finds that the resulting non-equilibrium fluxes induce both a growth of large droplets at the expense of small droplets and a net drift of droplets towards regions of low regulator concentration (high supersaturation). This is analogous to the segregation of P-granules at the posterior end of *C. elegans* zygotes.

3. Asymptotic analysis of Ostwald ripening in 2D

As we mentioned in the introduction, classical LSW theory breaks down in the case of circular droplets in two-dimensional systems, since the concentration around a droplet varies as $\ln R$ rather than R^{-1}. It is then necessary to use some form of matched asymptotics in order to handle the far-field behavior [15, 7]. Here we use such methods to analyze 2D droplet ripening in a regulator concentration gradient. In contrast to the previous analysis of 3D droplets [25, 26], the far-field ϕ_∞ is taken to be spatially uniform and is determined self-consistently in terms of an area preserving solvability condition; such a condition is typical of late-stage ripening. This is based on the separation of length-scales assumed in classical Ostwald ripening, whereby quasi-stationary fluxes between droplets can be maintained by a concentration profile that is approximately flat in the far field. (This corresponds to the outer solution of the matched asymptotic expansion.) It should be noted that such an argument holds whether or not droplets are uniformly distributed throughout the domain, and is not invalidated by the presence of a regulator concentration gradient. For the latter only affects the low density concentration (area fraction) ϕ_a in the boundary later around each droplet. As in classical LSW theory, we will also assume a separation of time-scales in which the growth and drift of droplets occurs on a much slower time-scale than diffusion. This means that we can solve the quasi-steady-state diffusion equation for the solute concentration ϕ. In section 4, we will use the resulting non-equilibrium fluxes to determine the droplet dynamics.

Consider N droplets of radii R_i and centers $\mathbf{x}_i$, $i = 1, \ldots, N$, located in a bounded 2D domain $\Omega \subset \mathbb{R}^2$. The basic assumption of the asymptotic method is that the droplets are small and well separated. We fix length scales by setting the mean separation $d = 1$ and take the capillary length $\ell_c = \epsilon$, $R_i = \epsilon \rho_i$ with $0 < \epsilon \ll 1$ such that $\rho_i = O(1)$ and $|\mathbf{x}_i - \mathbf{x}_j| = O(1)$ for $j \neq i$. Note that in order to use singular perturbation theory with ϵ treated as an expansion parameter, we require the size of the droplets to be much smaller than the size of the domain and the spacing between droplets, and to be comparable to the capillary length. The last condition is a particularly strong constraint of the analysis. For simplicity, the high density concentration ϕ_b is taken to be $\mathbf{x}$-independent so that we can focus on the concentration in the domain exterior to the droplets. Suppose that there is a regulator concentration gradient in the x-direction of the form $\phi_R(x) = \phi_R(0) - bx$, where b specifies the steepness of the gradient. Due to the dependence of the effective
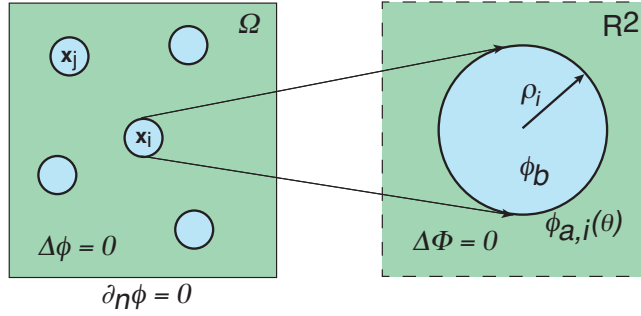
Figure 2: Construction of inner solution. The inner solution is expressed in terms of stretched coordinates $\boldsymbol{\rho}_i = \epsilon^{-1}(\mathbf{x} - \mathbf{x}_i)$, where $\mathbf{x}_i$ is the center of the i-th droplet. The rescaled radius is ρ_i and the region outside the droplet is taken to be $\mathbb{R}^2$ rather than the bounded domain Ω. The concentration inside the droplet is given by the constant ϕ_b, with a discontinuity at the interface so that $\Phi(\rho_i^+, \theta) = \phi_{a,i}(\theta)$.

interaction parameter χ_{eff} on $\phi_R(x)$, it follows that the low density equilibrium concentration $\phi_a(x)$ varies around the surface $|\mathbf{x} - \mathbf{x}_i| = \epsilon \rho_i$ of the i-th droplet. In particular, introducing the polar coordinates $x = x_i + \epsilon \rho_i \cos \theta$, $y = y_i + \epsilon \rho_i \sin \theta$ and setting $\phi_{a,i}(\theta) = \phi_a(x_i + \epsilon \rho_i \cos \theta)$, we obtain the leading-order Taylor expansion

$$\phi_{a,i}(\theta) \approx \alpha_i + \epsilon \beta_i \rho_i \cos \theta, \tag{3.1}$$

with $\alpha_i = \phi_a(x_i)$ and $\beta_i = \phi_a'(x_i)$.

3.1. Inner solution

First, consider the inner solution around the ith droplet,

$$\Phi_i(\mathbf{y}) = \phi(\mathbf{x}_i + \epsilon \mathbf{y}), \quad \mathbf{y} = \epsilon^{-1}(\mathbf{x} - \mathbf{x}_i),$$

where we have introduced stretched coordinates and replaced the domain Ω by $\mathbb{R}^2$, see Fig. 2(a). It follows that

$$\frac{1}{\rho} \frac{\partial}{\partial \rho} \rho \frac{\partial \Phi_i}{\partial \rho} + \frac{1}{\rho^2} \frac{\partial^2 \Phi_i}{\partial^2 \theta} = 0 \text{ for } \rho_i < \rho < \infty, \tag{3.2}$$

with boundary condition

$$\Phi_i(\rho_i, \theta) = \phi_{a,i}(\theta) \left(1 + \frac{1}{\rho_i} \right). \tag{3.3}$$

The general solution of Laplace's equation in polar coordinates is of the form

$$\Phi_i(\rho, \theta) = A_{0,i} + B_{0,i} \ln \rho / \rho_i \tag{3.4}$$

$$+ \sum_{n=1}^{\infty} (A_{n,i} \rho^n + B_{n,i} \rho^{-n})[C_{n,i} \cos n\theta + D_{n,i} \sin n\theta].$$

On imposing the boundary condition, one finds that

$$\Phi_i(\rho, \theta) = \alpha_i \left(1 + \frac{1}{\rho_i} \right) + \nu B_i(\nu) \ln \rho / \rho_i + \epsilon \beta_i \rho_i \left(1 + \frac{1}{\rho_i} \right) \frac{\rho_i}{\rho} \cos \theta. \tag{3.5}$$

(All coefficients $A_{n,i}$ for $n \geq 1$ must vanish, otherwise we cannot match with the outer solution.) We have introduced the small parameter

$$\nu = -1/\ln \epsilon, \tag{3.6}$$

and for convenience have set $B_{0,i} = \nu B_i(\nu)$. The coefficients $B_i(\nu)$, $i = 1, \ldots, N$, can be determined by matching the inner solutions with the outer solution (see below). The presence of the small parameter ν rather than ϵ in the matched asymptotic expansion is a common feature of strongly localized perturbations in 2D domains. It is well-known that $\nu \to 0$ much more slowly than $\epsilon \to 0$. Hence, if one is interested in obtaining $O(\epsilon)$ accuracy, then it is necessary to sum over the logarithmic terms non-perturbatively. This can be achieved by matching the inner and outer solutions using Green's functions [23], which is equivalent to calculating the asymptotic solution for all terms of $O(\nu^k)$ for any k.

3.2. Matching with the outer solution

The outer solution is obtained by treating each droplet as a point source/sink, see Fig. 3. The resulting time-independent diffusion equation takes the form

$$\nabla^2 \phi = 0, \quad \mathbf{x} \in \Omega \backslash \{\mathbf{x}_1, \ldots, \mathbf{x}_N\}, \quad \partial_n \phi = 0, \quad \mathbf{x} \in \partial\Omega, \tag{3.7}$$

together with the matching condition

$$\phi \sim \alpha_j \left(1 + \frac{1}{\rho_j}\right) + B_j(\nu) + \nu B_j(\nu)[\ln |\mathbf{x} - \mathbf{x}_j| - \ln \rho_j] \tag{3.8}$$

as $\mathbf{x} \to \mathbf{x}_j$. The next step is to introduce the 2D Neumann Green's function $G(\mathbf{x}, \mathbf{y})$, which is uniquely defined by [23]

$$\nabla^2 G = \frac{1}{|\Omega|} - \delta(\mathbf{x} - \mathbf{y}), \quad \mathbf{x} \in \Omega, \tag{3.9}$$

and

$$\partial_n G = 0 \text{ on } \partial\Omega, \quad \int_\Omega G(\mathbf{x}, \mathbf{y}) d\mathbf{x} = 0 \tag{3.10}$$

for fixed $\mathbf{y}$. Note that G can be decomposed as

$$G(\mathbf{x}, \mathbf{y}) = -\frac{\ln |\mathbf{x} - \mathbf{y}|}{2\pi} + R(\mathbf{x}, \mathbf{y}), \tag{3.11}$$

where R is the regular part of the Green's function. The latter is non-singular in the limit $\mathbf{x} \to \mathbf{y}$ and incorporates the effects of the boundary conditions. It vanishes when $\Omega = \mathbb{R}^2$. We now make the ansatz

$$\phi(\mathbf{x}) \sim \phi_\infty - 2\pi\nu \sum_{i=1}^N B_i(\nu) G(\mathbf{x}, \mathbf{x}_i) \tag{3.12}$$

for $\mathbf{x} \notin \{\mathbf{x}_j, j = 1, \ldots, N\}$ for some constant far-field ϕ_∞. Observe that for $\mathbf{x} \notin \{\mathbf{x}_j, j = 1, \ldots, N\}$,

$$\nabla^2 \phi(\mathbf{x}) \sim -2\pi\nu \sum_{i=1}^N B_i(\nu) \nabla^2 G(\mathbf{x}, \mathbf{x}_i) = -\frac{2\pi\nu}{|\Omega|} \sum_{i=1}^N B_i(\nu). \tag{3.13}$$

Hence, the outer solution satisfies the steady-state diffusion equation if and only if

$$\sum_{i=1}^N B_i(\nu) = 0. \tag{3.14}$$

As we will show in section 4, this condition ensures that the total area of the droplets is conserved, which is a typical feature of late-stage Ostwald ripening.
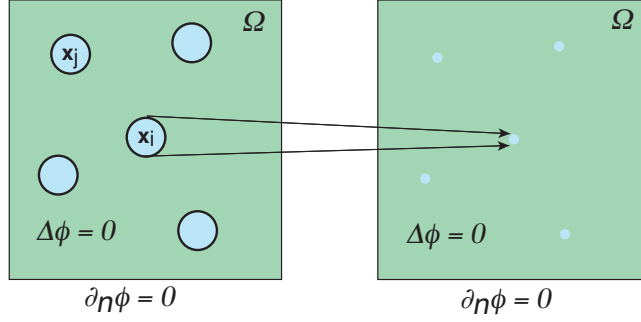
Figure 3: Construction of the outer solution ϕ. Each droplet is shrunk to a single point. The outer solution can be expressed in terms of the corresponding modified Neumann Green's function and then matched with the inner solution Φ around each droplet.

In order to match the inner and outer solutions, we note that as $\mathbf{x} \to \mathbf{x}_j$,

$$\phi(\mathbf{x}) \to \phi_\infty + \nu B_j(\nu) \ln |\mathbf{x} - \mathbf{x}_j| - 2\pi\nu B_j(\nu) R(\mathbf{x}_j, \mathbf{x}_j) - 2\pi\nu \sum_{i \neq j} B_i(\nu) G(\mathbf{x}_j, \mathbf{x}_i).$$

Comparison with the asymptotic limit in equation (3.8) yields the self-consistency conditions

$$-(1 - \nu \ln \rho_j + 2\pi\nu R(\mathbf{x}_j, \mathbf{x}_j)) B_j(\nu) - 2\pi\nu \sum_{i \neq j} B_i(\nu) G(\mathbf{x}_j, \mathbf{x}_i) = \alpha_j \left(1 + \frac{1}{\rho_j}\right) - \phi_\infty$$

$$(3.15)$$

for $j = 1, \ldots, N$. In particular, equation (3.15a) can be rewritten as a matrix equation

$$\sum_{i=1}^{N} (\delta_{i,j} + \nu M_{ji}) B_i(\nu) = \phi_\infty - \alpha_j \left(1 + \frac{1}{\rho_j}\right), \tag{3.16}$$

with

$$M_{jj} = 2\pi R(\mathbf{x}_j, \mathbf{x}_j) - \ln \rho_j, \; M_{ji} = 2\pi G(\mathbf{x}_j, \mathbf{x}_i), \; j \neq i. \tag{3.17}$$

We thus obtain the solution

$$B_i(\nu) = \sum_{j=1}^{N} [\mathbf{I} + \nu \mathbf{M}]_{ij}^{-1} \left(\phi_\infty - \alpha_j - \frac{\alpha_j}{\rho_j}\right), \tag{3.18}$$

which is clearly non-perturbative with respect to ν. However, for practical calculations, it is useful to Taylor expand $B_i(\nu)$ with respect to ν. This gives

$$B_i(\nu) = \phi_\infty - \alpha_i \left(1 + \frac{1}{\rho_i}\right) + \nu \sum_{j=1}^{N} M_{ij} \left[\phi_\infty - \alpha_j \left(1 + \frac{1}{\rho_j}\right)\right] + O(\nu^2). \tag{3.19}$$

3.3. Calculation of the far field ϕ_∞

It remains to determine ϕ_∞. Early on during phase separation, the fractional area of droplets is negligible, which suggests identifying ϕ_∞ with the local solute concentration in the absence of phase separation. This would imply that ϕ_∞ is itself space-dependent in the presence of a concentration gradient, see Refs. [25, 26]. In this paper we

assume that the area fraction of droplets reaches a steady-state as phase separation proceeds so that Ostwald ripening preserves the total area occupied by droplets. This is equivalent to imposing the area preserving condition (3.14), which in turn requires that ϕ_∞ is spatially uniform. If the latter did not hold, then equation (3.13) would have an additional term $\nabla^2 \phi_\infty$ on the right-hand side, and one could no longer ensure that $\sum_i B_i(\nu) = 0$. One would then need some information about the early-stages of droplet ripening. Equation (3.18) now implies that

$$\phi_\infty = \frac{\sum_{i,j=1}^{N} [\mathbf{I} + \nu \mathbf{M}]_{ij}^{-1} \alpha_j \left(1 + \frac{1}{\rho_j}\right)}{\sum_{i,j=1}^{N} [\mathbf{I} + \nu \mathbf{M}]_{ij}^{-1}}. \tag{3.20}$$

Hence, to leading order in ν,

$$\phi_\infty = N^{-1} \sum_{j=1}^{N} \alpha_j \left(1 + \frac{1}{\rho_j}\right) + O(\nu). \tag{3.21}$$

Note that in the absence of a regulator concentration gradient, $\alpha_i = \phi_a$ for all i, we have

$$\phi_\infty = \phi_a \left(1 + \frac{1}{\rho_{\mathrm{harm}}}\right) + O(\nu), \tag{3.22}$$

where ρ_{harm} is the harmonic mean,

$$\rho_{\mathrm{harm}} = \left[\frac{1}{N} \sum_{j=1}^{N} \frac{1}{\rho_j}\right]^{-1}. \tag{3.23}$$

(This is a major difference between classical droplet ripening in 2D and 3D, since in the latter case $\phi_\infty = \phi_a(1 + 1/\bar{\rho})$ with $\bar{\rho} = \sum_{i=1}^{N} \rho_i/N$.) Now substituting the leading order expression for the coefficients B_i into equations (3.5) and (3.12) shows that the concentration away from droplets (outer solution) is

$$\phi(\mathbf{x}) = \phi_\infty - 2\pi\nu \sum_{i=1}^{N} \left(\phi_\infty - \alpha_i - \frac{\alpha_i}{\rho_i}\right) G(\mathbf{x}, \mathbf{x}_i) + O(\nu^2), \tag{3.24}$$

whereas the inner solution near the i-th droplet with $|\mathbf{x} - \mathbf{x}_i| = \epsilon\rho$ is

$$\Phi_i(\rho, \theta) = \alpha_i \left(1 + \frac{1}{\rho_i}\right) + \nu \left(\phi_\infty - \alpha_i - \frac{\alpha_i}{\rho_i}\right) \ln(\rho/\rho_i)$$

$$+ \epsilon\beta_i\rho_i \left(1 + \frac{1}{\rho_i}\right) \frac{\rho_i}{\rho} \cos\theta + O(\nu^2). \tag{3.25}$$

4. Droplet dynamics

On longer time-scales, the droplets can grow, drift or deform due to the normal fluxes of solute at the interface modifying the location of the interface. The local displacement $\delta R_i(\theta, t)$ of the i-th interface is determined by the normal velocity v_i, which for a circular droplet is obtained by matching the influx of solute molecules into a surface

arc of length $ds_i = R_i d\theta$ with the local change in area. Assuming that $\phi_b \gg \phi_{a,i}$, we have

$$\phi_b v_i(\theta) ds_i = J_i(R_i, \theta) ds_i,$$

where $J_i(r, \theta) = D \nabla \Phi_i(r/\epsilon, \theta) \cdot \mathbf{e}_r$. (The flux inside the droplet vanishes as the concentration is approximately constant.) Hence,

$$v_i(\theta) = \frac{D}{\phi_b} \nabla \Phi_i(r/\epsilon, \theta) \cdot \mathbf{e}_r. \tag{4.1}$$

We thus have $\delta R_i(\theta, t) = v_i(\theta) \delta t$. We now rescale by setting $R_i = \epsilon \rho_i$ and $t = \epsilon^2 \tau$, so that

$$\delta \rho_i(\theta, \tau) = \frac{D}{\phi_b} \nabla \Phi_i(\rho_i, \theta) \cdot \mathbf{e}_\rho \delta \tau.$$

From equation (3.5), we have

$$\nabla \Phi_i(\rho, \theta) \cdot \mathbf{e}_\rho = \frac{\nu B_i(\nu)}{\rho_i} - \epsilon \beta_i \left(1 + \frac{1}{\rho_i}\right) \cos \theta. \tag{4.2}$$

with the coefficient $B_i(\nu)$ given by equation (3.18). Assuming that the droplet maintains an approximately spherical shape, we can define the change in radius according to

$$\delta \rho_i(\tau) = (2\pi)^{-1} \int_0^{2\pi} \delta \rho_i(\theta, \tau) d\theta.$$

That is,

$$\frac{d\rho_i}{d\tau} = \frac{D}{2\pi \phi_b} \int_0^{2\pi} \nabla \Phi_i(\rho_i, \theta) \cdot \mathbf{e}_\rho d\theta = \frac{D\nu B_i(\nu)}{\rho_i \phi_b}. \tag{4.3}$$

Multiplying both sides of equation (4.3) by ρ_i, summing over i and imposing the solvability condition (3.14) implies that

$$\frac{1}{2\pi} \sum_{i=1}^N \frac{dA_i}{d\tau} = \frac{D\nu}{\phi_b} \sum_{i=1}^N B_i(\nu) = 0,$$

where $A_i = \pi \rho_i^2$ is the (rescaled) area of the i-th droplet. Hence, equation (3.14) ensures that the total area of the droplets is conserved. If we now expand $B_i(\nu)$ according to equation (3.19), then we obtain the leading order dynamical equation

$$\frac{d\rho_i}{d\tau} = \frac{\nu D}{\phi_b \rho_i} \left[\phi_\infty - \alpha_i \left(1 + \frac{1}{\rho_i}\right)\right] + O(\nu^2), \tag{4.4}$$

which is almost identical to the expected formula for growth of a 2D droplet.

In the absence of a regulator concentration gradient, $\alpha_i = \phi_{a,0}$ for all i and $\phi_{a,0}$ constant, large droplets grow at the expense of small droplets until only one remains. This is classical Ostwald ripening in 2D. However, in the presence of a concentration gradient the local equilibria become $\alpha_i = \alpha_i(\tau) := \phi_a(x_i(\tau))$, with $x_i(\tau)$ the time-dependent x-coordinate of the i-th droplet. That is,

$$\delta x_i(\tau) = (2\pi)^{-1} \int_0^{2\pi} \delta \rho_i(\theta, \tau) \cos \theta d\theta,$$

which yields the drift speed

$$\frac{dx_i}{d\tau} = \frac{D}{2\pi \phi_b} \int_0^{2\pi} \nabla \Phi_i(\rho_i, \theta) \cdot \mathbf{e}_\rho \cos \theta \ d\theta = -\frac{\epsilon D}{2\phi_b} \beta_i \left(1 + \frac{1}{\rho_i}\right). \tag{4.5}$$

Recall that $\beta_i = \nabla\phi_a(\mathbf{x}_i) \cdot \mathbf{e}_x$ so sign(β_i) determines whether the regulator concentration increases or decreases with increasing x. Equation (4.5) thus implies that droplets drift down the regulator concentration gradient. For example, if $\phi_R(x)$ is a decreasing function of x, then droplets tend to move towards larger values of x. It follows that α_i becomes a decreasing function of τ as the i-th droplet moves to regions of lower regulator concentration.

Further simplification can be achieved by noting that in 2D there is a separation of time-scales between the $O(\nu)$ rate of growth and the $O(\epsilon)$ rate of drift. More specifically, since $\epsilon|\ln\epsilon| \to 0$ as $\epsilon \to 0$, we see that for sufficiently small ϵ and a shallow concentration gradient (small $|\beta_i|$) the drift is much slower than the growth. At a given time τ, droplets upstream of the concentration gradient have larger $\alpha_i(\tau)$ and are thus more likely to shrink than downstream droplets of the same size, see equation (4.4). It follows that on the $O(\nu)$ time-scale, downstream droplets will grow at the expense of upstream droplets. So even in the absence of drift, there will tend to be a higher concentration of growing droplets towards the right-hand boundary shown in Fig. 4. On the longer $O(\epsilon)$ time-scale, surviving upstream droplets will drift to the right and thus further contribute to segregation. Under the assumptions of the model, there are thus two separate mechanisms for segregation: a spatial gradient of local equilibria at given time τ, and a slow rightward drift of droplets. Once surviving droplets have reached one end of the domain, they will have the same local equilibria and normal Ostwald ripening will tend to occur, with the caveat that the droplets may no longer have $O(1)$ separation. Finally, it should be noted that the segregation mechanism in the case of a homogeneous far-field concentration ϕ_∞ differs from the mechanism considered previously for 3D droplets [25, 26]. In the latter case, segregation is driven by a spatio-temporal gradient in ϕ_∞ and a spatial gradient in ϕ_a. Consequently, one finds a right-moving dissolution boundary separating growing from shrinking droplets.
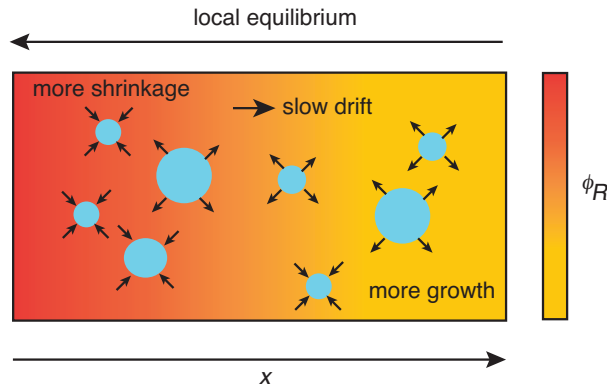

Figure 4: Droplet ripening in a regulator concentration gradient. The local equilibrium ϕ_a is larger for upstream droplets and hence there tends to be more shrinkage to the left compared to the right. Surviving droplets slowly drift to the right ultimately resulting in droplet segregation at the right-hand boundary.

4.1. Two droplets

In order to illustrate the effects of higher-order contributions to the coefficients $B_i(\nu)$ on droplet dynamics, we consider the case of two droplets in a circular domain. Since the $B_i(\nu)$ coefficients only appear in the growth dynamics, we ignore the effects of drift by taking the droplets to have the same low phase concentration $\alpha_1 = \alpha_2 = \phi_a$ and set $\beta_j = 0$. (This is a reasonable leading order approximation for 2D droplets when there is a separation of time scales between growth and drift as highlighted above.) The dynamics of the droplet radii can then be analyzed along identical lines to Ref. [15].

Let $\Omega \subset \mathbb{R}^2$ be the unit circle centered at the origin. (Take the radius $L = 1$ of the circle to determine the length-scale.) Suppose that there are two droplets $j = 1, 2$ in the interior of Ω with initial radii $R_j = \epsilon \rho_j$ and centers at $\mathbf{x}_j$. For concreteness, we take $\mathbf{x}_1 = (0, -1/2)$ and $\mathbf{x}_2 = (0, 2/3)$ with droplet 1 smaller than droplet 2, see Fig. 5(a). The Neumann Green's function for such a domain is well-known [15]:

$$G(\mathbf{x}, \mathbf{x}_j) = -\frac{1}{2\pi} \ln(|\mathbf{x} - \mathbf{x}_j|) + R(\mathbf{x}, \mathbf{x}_j)$$

$$= \frac{1}{2\pi}\left[-\ln(|\mathbf{x} - \mathbf{x}_j|) - \ln\left(\left| \mathbf{x}|\mathbf{x}_j| - \frac{\mathbf{x}_j}{|\mathbf{x}_j|} \right| \right) + \frac{1}{2}(|\mathbf{x}|^2 + |\mathbf{x}_j|^2) - \frac{3}{4} \right]. \quad (4.6)$$

From equation (3.18) we see that for two droplets we have to invert the matrix

$$\mathbf{A} = \begin{pmatrix} 1 + 2\pi R_{11} - \ln\rho_1 & 2\pi G_{12} \\ 2\pi G_{21} & 1 + 2\pi R_{22} - \ln\rho_2 \end{pmatrix}, \quad (4.7)$$

where $G_{ij} = G(\mathbf{x}_i, \mathbf{x}_j)$ and $R_{jj} = R(\mathbf{x}_j, \mathbf{x}_j)$. It follows that

$$\mathbf{A}^{-1} = \Gamma^{-1} \begin{pmatrix} 1 + \nu(2\pi R_{22} - \ln\rho_2) & -2\pi\nu G_{12} \\ -2\pi\nu G_{21} & 1 + \nu(2\pi R_{11} - \ln\rho_1) \end{pmatrix}, \quad (4.8)$$

with

$$\Gamma = (1 + \nu[2\pi R_{11} - \ln\rho_1])(1 + \nu[2\pi R_{22} - \ln\rho_2]) - 4\pi^2\nu^2 G_{12}G_{21}.$$

Introducing a dimensionless time according to the rescaling

$$\tau \to \frac{\tau\nu D}{\phi_b L^2}$$

and setting $\phi_a = 1$, equation (4.4) can be rewritten as

$$\frac{d\rho_i}{d\tau} = \frac{B_i(\nu)}{\rho_i}, \quad B_i(\nu) = \sum_{j=1,2} A_{ij}^{-1} \left[\frac{1}{\rho_{\mathrm{harm}}} - \frac{1}{\rho_j} \right] \quad (4.9)$$

for $i = 1, 2$. Numerical simulation of the ODEs (4.9) establish that the larger droplet grows and the smaller droplet shrinks, while preserving the total droplet area. A comparison of the results based on the leading order expansion of $B_i(\nu)$ in equation (3.19) and the full non-perturbative expression in (3.18) is illustrated in Fig. 5(b).

Following Ref. [15], one can estimate the extinction time T of the smaller droplet using the leading order dynamics (4.4), which for a pair of droplets becomes

$$\frac{d\rho_j}{d\tau} = \frac{1}{\rho_j}\left[\frac{1}{\rho_{\mathrm{harm}}} - \frac{1}{\rho_j} \right]. \quad (4.10)$$

Suppose that $\rho_1(0) < \rho_2(0)$ as in Fig. 5. First note that

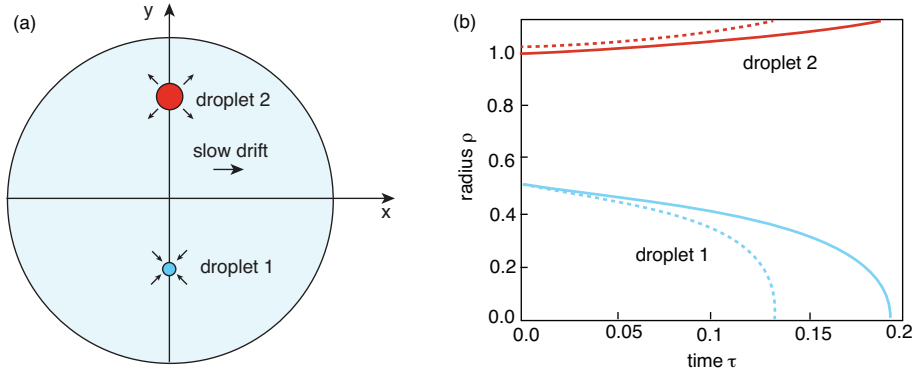$$\frac{d\rho_1}{d\tau} \geq -\frac{1}{\rho_1^2},$$

Figure 5: Pair of droplets. (a) Initial configuration of a pair of droplets at positions $\mathbf{x}_1 = (0, -1/2)$ and $\mathbf{x}_2 = (0, 2/3)$ with droplet 2 larger than droplet 1. (b) Example plots of the droplet radii $\rho_i(\tau)$, $i = 1, 2$, evolving according to equation (4.3) after non-dimensionalizing the time. Initial radii are $\rho_1(0) = 0.5$, $\rho_2(0) = 1$ and $\epsilon = 0.05$. Solid curves denote the solution based on the full non-perturbative expression for the coefficients $B_i(\nu)$, equation (3.18), whereas the dashed curves are based on the leading order approximation in equation (3.19). The larger droplet grows at the expense of the smaller droplet until the latter disappears after a finite time. On a slower time scale the droplets will drift down a regulatory concentration gradient in the x direction.

which on integrating with respect to time gives

$$\rho_1(\tau)^3 - \rho_1(0)^3 \geq -3\tau.$$

Hence, $\rho_1(\tau) \geq 0$ for all times $\tau \leq \rho_1(0)^3/3$, which yields a lower bound on the extinction time, namely, $T \geq \rho_1(0)^3/3$. Next, using the definition of the harmonic mean, we have

$$\rho_1^2 \frac{d\rho_1}{d\tau} = \rho_1 \left[\frac{1}{2\rho_2} + \frac{1}{2\rho_1} - \frac{1}{\rho_1} \right] = \frac{\rho_1}{2} \left[\frac{1}{\rho_2} - \frac{1}{\rho_1} \right] = \frac{\rho_1 - \rho_2}{2\rho_2} \leq \frac{\rho_1(0) - \rho_2(0)}{2\rho_2(0)} < 0$$

Again integrating with respect to time shows that

$$\rho_1(\tau)^3/3 - \rho_1(0)^3/3 \leq \frac{\rho_1(0) - \rho_2(0)}{2\rho_2(0)}\tau.$$

It follows that $\rho_1(\tau)$ is negative (extinct) for times

$$\tau \geq \frac{2\rho_1(0)^3\rho_2(0)}{\rho_2(0) - \rho_1(0)},$$

which yields an upper bound for the extinction time. In summary,

$$\frac{\rho_1(0)^3}{3} \leq T \leq \frac{2\rho_1(0)^3\rho_2(0)}{3[\rho_2(0) - \rho_1(0)]}. \tag{4.11}$$

For the plots shown in Fig. 5, we have $\rho_1(0) = 0.5$ and $\rho_2(0) = 1$ so that the extinction time under the leading-order approximation lies in the range $1/24 \leq T \leq 1/6$.

Fig. 5 suggests that the leading order approximation captures the qualitative growth/shrinkage of the droplets. However, there are significant errors in the extinction time. This reflects the fact that even though ϵ is small, $\epsilon = 0.05$, the actual expansion parameter $\nu = -1/\ln \epsilon \approx 1/3$. As we have already commented in section 3.1, the presence of the small parameter ν rather than ϵ is a common feature

of strongly localized perturbations in 2D domains. Therefore, in order to obtain $O(\epsilon)$ accuracy, it is necessary to sum over the logarithmic terms non-perturbatively as in equation (4.9). Finally note that in the presence of a regulator concentration gradient in the x direction, the droplets will slowly drift down the gradient. After non-dimensionalizing time, equation (4.5) becomes

$$\frac{dx_i}{d\tau} = -\frac{\epsilon\beta_i}{2\nu}\left(1+\frac{1}{\rho_i}\right) = -\frac{\epsilon\ln\epsilon|\beta_i|}{2}\left(1+\frac{1}{\rho_i}\right) > 0.$$

We are assuming that the regulator gradient is a decreasing function of x so $\beta_i < 0$. Note that for the value $\epsilon = 0.05$ used in Fig. 5, $-\epsilon\ln\epsilon \approx 0.15$ so that the rate of drift is an order of magnitude slower than the growth/shrinkage of the droplets as given by equation (4.9). In the analysis of 3D droplets [25, 26], it was shown how relatively fast segregation of droplets to one end of the concentration gradient could lead to periods of transient arrest, during which the number and size of droplets remains approximately constant. This was preceded by a narrowing of the droplet size distribution. The separation of time-scales that occurs in the case of 2D droplets suggests that this effect could be inhibited.

5. Discussion

In this paper we used asymptotic methods to investigate the ripening of 2D droplets in a regulator concentration gradient, which cannot be analyzed using classical LSW mean field theory. One major assumption of our asymptotic analysis, which contrasts with the previous analysis of 3D droplets [25, 26], is that the far-field solute concentration ϕ_∞ is spatially uniform. Mathematically speaking, this is a consequence of the solvability condition (3.14), which determines ϕ_∞ according to equation (3.20). From a physical perspective, we are exploiting a separation of length-scales as in classical late-stage Ostwald ripening, whereby quasi-stationary fluxes between droplets can be maintained by a concentration profile that is approximately flat in the far field (the outer solution of our asymptotic analysis). Two additional assumptions of our analysis are that the droplets are well separated and comparable in size to the capillary length ℓ_c, so it would break down in the case of densely populated large droplets whose size differ considerably from ℓ_c.

The main result of our asymptotic analysis was to identify a possible mechanism for segregation of 2D droplets in the presence of a regulator concentration gradient and a homogeneous far field ϕ_∞. Exploiting a separation of time-scales between droplet growth/shrinkage and drift, we showed that there are two distinct mechanisms for segregation: a spatial gradient in the local equilibria $\phi_a(x)$, which tends to favor the growth of downstream droplets, and a slow rightward drift of surviving droplets. The time course of segregation thus appears to differ from the model of 3D droplets [25, 26]. However, this reflects the fact that we are considering segregation during late-stage Ostwald ripening, assuming that the latter can be reached. It is a non-trivial problem to analyze the time-dependent diffusion process associated with earlier stages of segregation in 2D. At the very least, we have established that segregation is consistent with late-stage Ostwald ripening.

One distinctive feature of 2D compared to 3D droplets, which holds whether or not there is a concentration gradient, is that the matched asymptotics involves an expansion in the small parameter $\nu = -1/\ln\epsilon$ rather than ϵ. Hence, in order to obtain $O(\epsilon)$ accuracy, it is necessary to sum all logarithmic terms non-perturbatively using

Green's functions [23]. Analogous 2D singular perturbation problems arise in many other application areas, such as first passage time problems for Brownian motion in a domain with small traps [9, 8, 24] and diffusion-limited reaction rates in the case of small targets [21, 6]. These latter studies also reduce the associated boundary value problem to an $N \times N$ linear system of equations, similar in form to equations (3.15), where N is now the number of targets. Solving the linear equations numerically yields a non-perturbative solution that matches well with direct simulations of the full system for small ϵ. Although we did not simulate the full system in this paper, we expect similar agreement to hold. Here we focused instead on extracting general information about the system by carrying out a regular perturbation expansion in ν. In particular, we recovered droplet growth dynamics similar in form to classical theory, see equation (4.4). We also showed that the critical radius for droplet growth depends on the local supersaturation $\phi_\infty - \phi_a(\mathbf{x}_i)$, with ϕ_∞ given by a weighted harmonic mean of the droplet radii; this is distinct from 3D droplets where ϕ_∞ depends on the arithmetic mean. Including higher-order contributions to the droplet dynamics then allowed us to take account of finite-size effects associated with the boundary of the domain and the positions of the droplets, as determined by the associated Neumann Green's function. Thus, even a regular perturbation expansion in ν allows us to include the effects of droplet interactions that are neglected in mean field approaches. As illustrated in Fig. 5(b) for a pair of droplets, such interactions effect the extinction time of the small droplet. For the chosen configuration, the extinction time was increased. It would be interesting to investigate whether or not such a result holds in the case of multiple droplets and other geometries.

We end by making a few comments about possible biological implications of our analysis. The main challenge experimentally is to find a cellular preparation that exhibits biological condensation in a quasi-2D system. As we mentioned in the introduction, two potential candidates are curvature-inducing proteins in the plasma membrane that regulate cell shape [13], and polarized crawling cells such as keratocytes and fibroblasts that are highly flattened. One would then need to identify an appropriate regulator protein concentration gradient. Our modeling and analysis would predict that there is segregation of droplets along the regulator concentration gradient, although the time course of segregation may differ from the 3D case. In particular, our analysis suggests that there is a separation of time-scales between the growth and drift of droplets with the former occurring at a rate of $O(\nu)$ and the latter at a rate of $O(\epsilon)$, where ϵ is the characteristic size of a droplet relative to the domain size.

References

[1] Alikakos N D, Fusco G and Karali G 2004 Ostwald ripening in two dimensions – the rigorous derivation of the equations from the Mullins-Sekerka dynamics *J. Diff. Eqs.* **205** 1-49

[2] Banani S F, Lee H O, Hyman A A and Rosen M K 2017 Biomolecular condensates: organizers of cellular biochemistry. *Nat. Rev. Mol. Cell Biol.* **18** 285-298

[3] Berry J, Brangwynne C P and Haataja H P 2018 Physical principles of intracellular organization via active and passive phase transitions *Rep. Prog. Phys.* **81** 046601

[4] Brangwynne C P et al. 2009 Germline P granules are liquid droplets that localize by controlled dissolution/condensation *Science* **324** 1729-1732

[5] Brangwynne C P, Mitchison T J and Hyman A A 2011 Active liquid-like behavior of nucleoli determines their size and shape in Xenopus laevis oocytes *Proc. Natl Acad. Sci.* **108** 4334-4339

[6] Bressloff P C and Lawley S D 2015 Stochastically-gated diffusion-limited reactions for a small target in a bounded domain. *Phys. Rev. E* **92** 062117.

[7] Bressloff P C 2020 Active suppression of Ostwald ripening: beyond mean field theory *Phys. Rev. E* **101** 042804

[8] Cheviakov A F and Ward M J 2011 Optimizing the principal eigenvalue of the laplacian in a sphere with interior traps. *Math. Comp. Modeling* **53** 042118.

[9] Coombs D, Straube R and Ward M 2009 Diffusion on a sphere with localized traps: Mean first passage time, eigenvalue asymptotics, and Fekete points. *SIAM J. Appl. Math.* **70** 302-332.

[10] Doi D 2013 *Soft Matter Physics.* Oxford University Press, Oxford

[11] Elbaum-Garfinkle S et al 2015 The disordered P granule protein LAF-1 drives phase separation into droplets with tunable viscosity and dynamics *Proc. Natl. Acad. Sci. USA* **112** 7189-7194

[12] Falahati H and Haji-Akbari A 2019 Thermodynamically driven assemblies and liquid-liquid phase separations in biology *Soft Matter* **15** 1135-1154

[13] Gov N S 2018 Guided by curvature: shaping cells by coupling curved membrane proteins and cytoskeletal forces *Roy. Soc. Phil Trans. B* **373** 20170115

[14] Hyman A A, Weber C A and Julicher F 2014 Liquid-liquid phase separation in biology *Annu. Rev. Cell Dev. Biol.* **30** 39-58

[15] Kavanagh E 2014 Interface motion in the Ostwald ripening and chemotaxis systems. Master Thesis, University of British Columbia

[16] Lee C F, Brangwynne C P, Gharakhani J, Hyman A A and Julicher F 2013 Spatial organization of the cell cytoplasm by position-dependent phase separation *Phys. Rev. Lett.* **111** 088101

[17] Lee C F and Wurtz J D 2019 Novel physics arising from phase transitions in biology *J. Phys. D* **52** 023001

[18] Lifshitz I M and Slyozov V V 1961 The kinetics of precipitation from supersaturated solid solutions *J. Phys. Chem. Solids.* **19** 35-50

[19] Ostwald W 1897 *Z. Phys. Chem* **22** 289

[20] Saha S et al 2016 Polar positioning of phase-separated liquid compartments in cells regulated by an mRNA competition mechanism *Cell* **166** 1572-1584

[21] Straube R, Ward M J and Falcke M 2007 Reaction rate of small diffusing molecules on a cylindrical membrane. *J. Stat. Phys.* **129** 377-405

[22] Wagner C 1961 Theorie der Alterung von Niederschlägen durch Umlösen *Z. Elektrochemie* **65** 581-594

[23] Ward M J, Henshaw W D and Keller J B 1993 Summing logarithmic expansions for singularly perturbed eigenvalue problems *SIAM J. Appl. Math* **53** 799-828

[24] Kurella V, Tzou J C, Coombs D and Ward M J 2015 Asymptotic analysis of first passage time problems inspired by ecology. *Bull Math Biol.* **77** 83-125.

[25] Weber C A, Lee C F and Jülicher F 2017 Droplet ripening in concentration gradients *New J. Phys.* **19** 053021

[26] Weber C A, Zwicker D, Jülicher F and Lee C F 2019 Physics of active emulsions *Rep. Prog. Phys.* **82** 064601

[27] Wurtz J D and Lee C F 2018 Chemical-reaction-controlled phase separated drops: formation, size selection and coarsening *Phys. Rev. Lett.* **120** 078102

[28] Zwicker D, Decker M, Jaensch S, Hyman A A and Jülicher F 2014 Centrosomes are autocatalytic drops of pericentriolar material organized by centrioles *Proc. Natl Acad. Sci. USA* **111** E2636-2645

[29] Zwicker D, Hyman A A and Jülicher F 2015 Suppression of Ostwald ripening in active emulsions *Phys. Rev. E* **92** 012317